PAPER

Check for updates

Modeling molecular ensembles with gradient-domain machine learning force fields†

Alex M. Maldonado, [a] Igor Poltavsky, [b] Valentin Vassilev-Galindo, [bc] Alexandre Tkatchenko *[b] and John A. Keith *[a]

Gradient-domain machine learning (GDML) force fields have shown excellent accuracy, data efficiency, and applicability for molecules with hundreds of atoms, but the employed global descriptor limits transferability to ensembles of molecules. Many-body expansions (MBEs) should provide a rigorous procedure for size-transferable GDML by training models on fundamental n-body interactions. We developed many-body GDML (mbGDML) force fields for water, acetonitrile, and methanol by training 1-, 2-, and 3-body models on only 1000 MP2/def2-TZVP calculations each. Our mbGDML force field includes intramolecular flexibility and intermolecular interactions, providing that the reference data adequately describe these effects. Energy and force predictions of clusters containing up to 20 molecules are within 0.38 kcal mol^{-1} per monomer and 0.06 kcal (mol Å)$^{-1}$ per atom of reference supersystem calculations. This deviation partially arises from the restriction of the mbGDML model to 3-body interactions. GAP and SchNet in this MBE framework achieved similar accuracies but occasionally had abnormally high errors up to 17 kcal mol^{-1}. NequIP trained on total energies and forces of trimers experienced much larger energy errors (at least 15 kcal mol^{-1}) as the number of monomers increased—demonstrating the effectiveness of size transferability with MBEs. Given these approximations, our automated mbGDML training schemes also resulted in fair agreement with reference radial distribution functions (RDFs) of bulk solvents. These results highlight mbGDML's value for modeling explicitly solvated systems with quantum-mechanical accuracy.

1 Introduction

Machine learning (ML) potentials and force fields[1–3] have revolutionized atomistic modeling by facilitating larger and longer simulations crucial for modeling dynamic and kinetic properties.[4,5] General-purpose ML potentials (*e.g.*, ANI-2x,[6] OrbNet Denali,[7] AIQM1 [8]) model chemical (local) interactions and can be useful for subsets of chemical space. These approaches assist molecular screening but require enormous data sets of hundreds of thousands of structures. Alternatively, ML potentials can be tailored to specific systems to improve desired simulation reliability. This requires that models be retrained for each system, so training must involve minimal human involvement and computations to be practical.

Size transferability to hundreds of molecules is paramount for useful ML potentials. Most ML potentials rely on local descriptors[9–12] or graph neural networks (GNNs)[13,14] that partition total properties into atomic contributions. Local descriptors have been successful in numerous applications, but they inherently neglect or limit complicated non-local interactions by enforcing atomic radial cutoffs. For example, a recent study showed that a deep neural network potential's predictions of liquid water properties are sensitive to training data relevant to the thermodynamic state point.[15] Global descriptors (such as the Coulomb matrix and pairwise atomic distances) impose no such constraints and capture interactions at all scales.[16,17] Still, they are usually restricted to the same number of atoms.

Gradient-domain ML (GDML) uses a global descriptor and has demonstrated remarkable success in many chemical applications with monomers or dimers.[18–22] Moreover, GDML only needs energies and forces of approximately 1000 structures to accurately learn the potential energy surfaces of molecules[19] and periodic materials.[17] The global descriptor limits GDML to the same system it was trained on, whether a single molecule or a chemical reaction. Size-transferable GDML for molecular ensembles would provide rapidly trained force fields for high-quality molecular simulations involving solvents.

Many-body expansions (MBEs) should enable size-transferable GDML because systems with non-covalent clusters are naturally described in terms of n-body interactions.[23,24] Data-driven, many-body potentials (*e.g.*, MB-pol) have already

[a]Department of Chemical and Petroleum Engineering, University of Pittsburgh, Pittsburgh, Pennsylvania 15260, USA. E-mail: jakeith@pitt.edu

[b]Department of Physics and Materials Science, University of Luxembourg, L-1511 Luxembourg City, Luxembourg. E-mail: alexandre.tkatchenko@uni.lu

[c]IMDEA Materials Institute, C/Eric Kandel 2, 28906 Getafe, Madrid, Spain

† Electronic supplementary information (ESI) available. See DOI: https://doi.org/10.1039/d3dd00011g

been widely successful in modeling aqueous systems.[25–27] This expansion is formally exact if all N-body interactions are accounted for with sufficient accuracy and precision. However, the expansion is typically truncated to the third order due to combinatorics. One can avoid truncating the expansion and include all contributions by using a classical many-body polarization model (*e.g.*, a Thole-type model as in MB-pol[25]). We expect training on fundamental n-body interactions found in clusters would extend GDML force fields to be useful for bulk liquid simulations. Alternative approaches exist; for example, Gaussian Approximation Potential (GAP)[3,11] was extended to liquid methane by decomposing energies into fundamental interactions (*e.g.*, repulsion, dispersion, and electrostatic contributions) and different length scales.[28] This is another rigorous approach that requires considerable effort with large numbers of quantum chemical calculations.

MBEs share characteristics with local descriptors but provide several key advantages. First, n-body interactions are more efficiently treated on a molecular basis instead of an atomic basis. Second, errors associated with MBE truncation can be corrected using a variety of schemes. For example, using long-range physical models to capture induction and dispersion effects.[29,30] Alternatively, one could use ONIOM-style[31] approaches such as molecules-in-molecules (MIM)[32] and molecular tailoring approach (MTA)[33] where low-cost calculations on the whole structure (*i.e.*, supersystem) are used to capture all long-range interactions. Third, these n-body contributions can be observed in relatively small clusters. Local descriptors require data on large clusters to achieve similar levels of size transferability.[34] This opens the door for many-body GDML (mbGDML) force fields trained on high levels of theory that scale poorly with system size, such as CCSD(T). In addition, mbGDML naturally incorporates intramolecular/monomer flexibility, which is extremely challenging for analytical potentials.

Thus, mbGDML should provide size-transferable force fields trained on highly accurate quantum chemical methods. To evaluate this, we developed an automated framework in Python to facilitate training and application of mbGDML force fields (available at **https://github.com/keithgroup/mbGDML**). GDML force fields for water (H_2O), acetonitrile (MeCN), and methanol (MeOH) were trained on 1000 structures for 1-, 2-, and 3-body interactions. GAP and SchNet[35] were also evaluated in this many-body framework. The size transferability of mbGDML was further assessed against a highly promising graph neural network, Neural Equivariant Interatomic Potentials (NequIP).[13] Reference structures from the literature were used to benchmark energy and forces predictions. The following sections demonstrate mbGDML energy and force accuracies within 0.38 kcal mol^{-1} per monomer and 0.06 kcal (mol Å)$^{-1}$ per atom for structures containing up to 20 monomers (120 atoms). The MBE framework itself contributes 14% to 83% of these errors depending on the system. Error cancellation dramatically improves relative energy predictions of mbGDML to less than 3 kcal mol^{-1} and achieves fair to excellent agreement with solvent radial distribution functions (RDFs).

2 Methods

The MBE represents the total system energy, E, composed of N noncovalently connected (*i.e.*, non-intersecting) fragments as the sum of n-body interaction energies:[36]

$$E = \sum_i^N E_i^{(1)} + \sum_{i<j}^N \Delta E_{ij}^{(2)} \sum_{i<j<k}^N \Delta E_{ijk}^{(3)} + \dots \quad (1)$$

Here, N is the number of monomers; i, j, k are monomer indices; $E_i^{(1)}$ is the energy of monomer i; and $\Delta E_{i,j,\dots}^{(n)}$ represents the n-body interaction energy contribution of the fragment containing monomers $i, j, \dots$ with lower order ($<n$) contributions removed. For example, the 2-body contribution of the fragment containing monomers i and j is

$$\Delta E_{ij}^{(2)} = E_{ij}^{(2)} - E_i^{(1)} - E_j^{(1)} \quad (2)$$

and the 3-body contribution with monomers i, j, and k are

$$\Delta E_{ijk}^{(3)} = E_{ijk}^{(3)} - \Delta E_{ij}^{(2)} - \Delta E_{ik}^{(2)} - \Delta E_{jk}^{(2)} \\ - E_i^{(1)} - E_j^{(1)} - E_k^{(1)} \quad (3)$$

Eqn (1) is exact when all n-body contributions up to N are accounted for with exact accuracy and precision. This equation also holds for properties expressed as a derivative of energy (*i.e.*, gradients).

The xTB program[37] v6.4.0 was used to run molecular dynamics (MD) simulations of the three solvents at 500 K. Small clusters containing up to three molecules were sampled from these simulations to generate data sets for training. Higher temperatures provided configurations relevant at lower temperatures with the added benefit of sampling high-energy regions.[2] GFN2-xTB,[38] a semiempirical quantum mechanics method, was used as a compromise between the cost of quantum chemical methods and potentially not having classical force field parameters for species of interest. Furthermore, simulation accuracy is not a significant concern because only reasonable geometries are desired at this stage.

Eqn (1) represents the MBE framework where individual GDML force fields are trained on intramolecular (*i.e.*, 1-body) and intermolecular (*i.e.*, 2- and 3-body) energies and forces. Energies and forces were calculated with ORCA v4.2.0 (ref. 39 and 40) using second-order Møller–Plesset perturbation (MP2) theory,[41] the def2-TZVP basis set,[42] and the frozen core approximation. This level of theory was chosen for its efficiency and accuracy for noncovalent interactions, but future applications of mbGDML are recommended to use the highest levels of quantum chemical theory available for training data. The Resolution of Identity (RI) approximation was only used for calculations containing 16 or more monomers. Additional calculation details and discussion can be found in the ESI.†

3 Results and discussion

3.1 Small isomers

We evaluated mbGDML, mbGAP, and mbSchNet on tetramers (4mers), pentamers (5mers), and hexamers (6mers) from the

---

literature.[43–45] These test structures have minimal higher-order (>3-body) contributions that increase with the number of monomers. Furthermore, many-body ML (mbML) potentials considered here implement a distance-based cutoff for 2- and 3-body contributions (see the ESI for more details†). Small clusters allow us to determine whether errors are from the underlying MBE framework or ML predictions.

ML potentials discussed here are trained on small data sets of only 1000 structures to showcase GDML data efficiency. Training sets were determined through an iterative training procedure to reduce the maximum model error.[46] GAP and SchNet models were trained on the same training sets as GDML for a fair comparison. In theory, training sets could be tailored for GAP and SchNet to reduce errors; however, a cursory attempt

did not substantially improve results. We reiterate that GAP and SchNet normally require substantially large training sets. In other words, GAP and SchNet potentials presented here are technically underfitted compared to standard practices. More information can be found in the ESI.†

Fig. 1 shows relative isomer energies with respect to the lowest energy structure for MBE (light color) and mbGDML (dark color) methods. The ESI† provides comparable figures for mbGAP and mbSchNet. Figures showing absolute energy predictions for these structures are also shown in the ESI† and help determine where error cancellation comes into play. First, we discuss the inherent errors in MBE data *versus* supersystem MP2 data (gray). These MBE predictions generally capture the relative energy trends of water, acetonitrile, and methanol
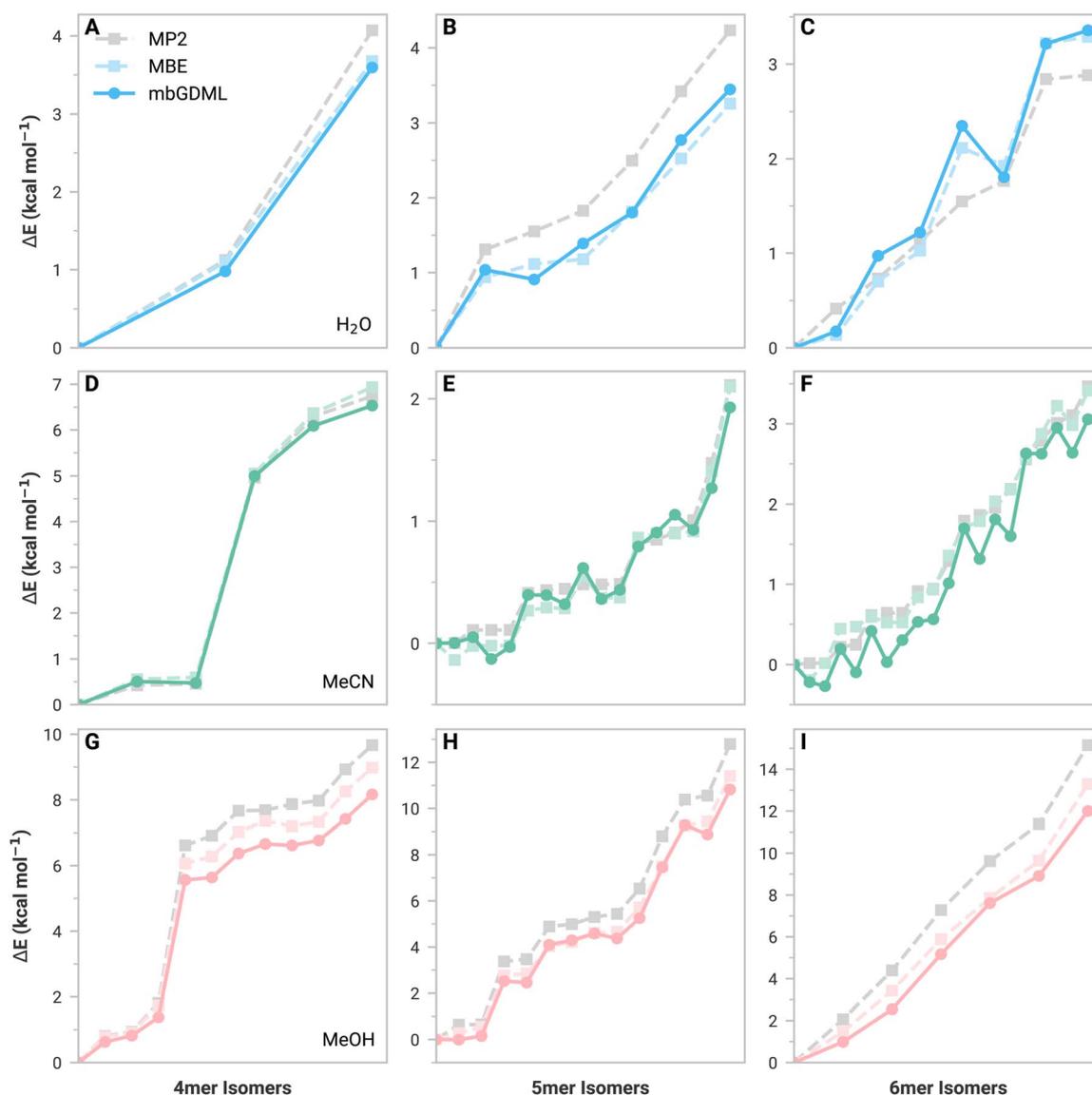

Fig. 1 Relative energies of isomers containing four, five, and six monomers of (A–C) water, (D–F) acetonitrile, and (G–I) methanol. Gray dashed lines are the reference MP2/def2-TZVP calculations. Light-colored lines with squares are MBE predictions calculated with MP2/def2-TZVP with no distance-based cutoffs for 2- and 3-body predictions. Dark-colored lines with circles are mbGDML predictions. Different y-axis scales are used for each subplot to enhance visualization.

isomers. Water predictions showed increasing errors with system size, indicating the importance of higher-order contributions (as expected). Acetonitrile 5mers and 6mers (Fig. 1D–F) show small energy differences that are not monotonically increasing. This is likely due to challenging electrostatics and polarization from dipole–dipole interactions. Methanol isomer MBE predictions showed this same trend as water, but higher-energy structures now exhibit lower MBE errors. This suggests that higher-order contributions are crucial for stabilizing low-energy methanol structures. Incomplete basis sets and basis set superposition errors (BSSE) are known to impact MBE accuracy.[47–52] The def2-TZVP basis set was chosen for its balance of cost and accuracy, as the larger aug-cc-pVTZ basis set only improved the energy MAE by 0.15 kcal mol^{-1}. BSSE corrections are not included here because the n-body energies and forces would depend on the original supersystem—thereby limiting data set transferability.

We now discuss mbGDML data, which approximates the MBE potential energy surface. In general, mbGDML reasonably mimics MBE data, including innate errors made by the MBE framework, as seen in the acetonitrile 5mer and 6mer data. Note that fortuitous error cancellations of 2- and 3-body mbGDML predictions sometimes give the appearance of higher accuracy than MBE. mbGAP and mbSchNet potentials occasionally are better or worse than mbGDML; however, as previously mentioned, these methods generally require larger training sets and are likely to underperform here. For example, Table 1 shows the MBE, mbGDML, mbGAP, and mbSchNet energy and force mean absolute errors (MAEs) with respect to supersystem MP2/def2-TZVP calculations for all 4-6mer structures considered here. All mbML models perform similarly for water and acetonitrile, but the methanol isomer errors for mbGAP and mbSchNet are nearly double that for mbGDML.

Previous studies also investigated mbML models for water. Nguyen *et al.* use permutationally invariant polynomials (PIPs), Behler–Parrinello neural networks (BPNNs), and GAP models for predicting water 1, 2-, and 3-body interactions.[53] Their 2-body training set included 34 431 structures containing the global dimer minimum, saddle points, artificially compressed geometries, and geometries from path-integral molecular dynamics (PIMD) simulations using HBB2-pol.[54] Their 3-body

Table 2 Energy MAEs (kcal mol^{-1}) for 2- and 3-body interactions of small water isomers (4–6mers) from Fig. 1A–C. Reference data were computed with MP2/def2-TZVP. Best ML potential values are bolded

n-body	Training set	Method	4mers	5mers	6mers
2	1000	GDML	0.030	0.047	0.035
	1000	GAP	0.014	0.012	0.015
	1000	SchNet	**0.013**	**0.012**	**0.013**
	34 431[a]	PIP	0.050	0.054	0.145
	34 431[a]	BPNN	0.057	0.033	0.061
	34 431[a]	GAP	0.043	0.040	0.138
3	1000	GDML	0.093	0.071	0.041
	1000	GAP	0.134	0.129	0.112
	1000	SchNet	0.098	0.059	0.041
	10 001[a]	PIP	0.050	0.056	0.095
	10 001[a]	BPNN	0.040	0.070	0.123
	10 001[a]	GAP	**0.007**	**0.024**	**0.030**

[a] Data from ref. 53.

training set contained 10 001 structures from HBB2-pol MD and PIMD of small water clusters, liquid water, and ice phases. Table 2 shows 2- and 3-body interaction energy MAEs with their models and those calculated here. The PIP, BPNN, and GAP water models trained on large data sets achieved 2- and 3-body interaction energy MAEs on the order of 0.033–0.145 and 0.007–0.123 kcal mol^{-1}, respectively. Alternatively, our GDML force fields trained on only 1000 structures achieved MAEs of 0.030–0.047 and 0.041–0.093 kcal mol^{-1} for 2- and 3-body interaction energies. This shows that GDML models using small training sets can perform similarly to well-trained potentials requiring large training sets.[53] We highlight that the GAP results from ref. 53 demonstrate substantial accuracy improvements are possible with more extensive training sets.

We reiterate that ML potential accuracy is intricately linked to reference data sets, but we specifically opted to show the promise of GDML with small training sets. In almost all cases, the water 2-body models prepared here outperformed those from ref. 53 that used larger training sets. Presumably, our smaller data sets may contain structures that enhance the perceived accuracy of these models. The 3-body data exhibit the opposite trend, which can be attributed to data set quality. In general, additional sampling of configurational spaces would improve our mbML models; however, the objective here is to evaluate ML potentials that can be trained with minimal computational cost.

3.2 16mers

Predictions of medium-sized structures provide a straightforward test of size transferability. There are additional, albeit typically small, higher-order contributions in larger structures. Also, the n-body cutoffs are now in effect to reduce the number of computations. Table 3 shows energies and forces of hexadecamers (16mers) from the literature[55–57] computed with RI-MP2/def2-TZVP and compared against mbGDML, mbGAP, and mbSchNet results. The truncated MBE contributes a few-kcal mol^{-1} errors depending on the system. For example, the MBE prediction of $(H_2O)_{16}$ results in a 3.3 kcal mol^{-1} error

Table 1 Energy (kcal mol^{-1}) and force [kcal (mol Å)$^{-1}$] MAEs of 4–6mer predictions. MAEs on an energy/monomer and force/atom basis are italicized. Best ML potential values are bolded. Energy and forces are abbreviated as E and F, respectively

Method	H$_2$O		MeCN		MeOH	
	E	F	E	F	E	F
MBE	0.925	0.426	0.110	0.019	0.503	0.157
	0.169	*0.026*	*0.020*	*0.001*	*0.100*	*0.005*
mbGDML	1.340	0.737	0.296	**0.164**	**1.667**	**0.872**
	0.248	*0.045*	*0.057*	***0.005***	***0.342***	***0.030***
mbGAP	1.906	1.014	**0.264**	0.235	2.908	1.369
	0.345	*0.062*	***0.049***	*0.007*	*0.600*	*0.046*
mbSchNet	**1.285**	**0.690**	0.368	0.168	3.138	1.177
	0.237	*0.043*	*0.070*	*0.005*	*0.648*	*0.040*

Table 3 MBE and mbML absolute energy errors (kcal mol⁻¹) and force MAEs [kcal (mol Å)⁻¹] of 16mers with respect to RI–MP2/def2–TZVP. Errors on an energy/monomer and force/atom basis are italicized. Best ML potential values are bolded. Energy and forces are abbreviated as E and F, respectively

Method	$(H_2O)_{16}$		$(MeCN)_{16}$		$(MeOH)_{16}$	
	E	F	E	F	E	F
MBE	3.320	0.456	0.243	0.067	1.589	0.262
	0.207	*0.010*	*0.015*	*0.001*	*0.099*	*0.003*
mbGDML	4.013	0.903	**0.282**	**0.239**	5.561	1.070
	0.251	*0.019*	***0.018***	***0.002***	*0.348*	***0.011***
mbGAP	**3.749**	1.105	6.741	0.614	17.580	1.789
	0.234	*0.023*	*0.421*	*0.006*	*1.099*	*0.019*
mbSchNet	4.560	**0.767**	16.066	0.552	**3.422**	1.189
	0.285	***0.016***	*1.004*	*0.006*	***0.214***	*0.012*

whereas $(MeCN)_{16}$ has only a 0.2 kcal mol⁻¹ error. Missing higher-order contributions or basis set errors are the most likely causes. All mbML models performed similarly well with $(H_2O)_{16}$. Most errors originated from 3-body predictions, with error cancellation improving model performance.

3.2.1 Analysis of $(MeCN)_{16}$. We find that both mbSchNet and mbGAP models trained from smaller data sets have abnormally high errors for $(MeCN)_{16}$ and $(MeOH)_{16}$, respectively. In both cases, the 3-body model has substantial error accumulation. Cutoffs are not the issue because only −0.006 of the 16.1 kcal mol⁻¹ error in mbSchNet's prediction of $(MeCN)_{16}$ is from cutoffs implemented in the 2- and 3-body models. Prediction errors contribute the most; a massive −15.2 kcal-mol⁻¹ error comes from the 3-body SchNet model.

Assessing inadequacies of training data is more complicated. If 3-body structures from $(MeCN)_{16}$ are substantially different from the data sets, then the model may break down. To investigate this, we used dimensionality reduction to

visualize high-dimensional similarity in 2D space. Similar structures in feature space should be clustered together and *vice versa*.

Fig. 2A shows the GDML feature space, a 2D embedding of trained and 3-body structures from $(MeCN)_{16}$ using Uniform Manifold Approximation and Projection (UMAP).[58] There is a significant overlap between the GDML training set feature space and the structures from $(MeCN)_{16}$. High overlap suggests that GDML should have low prediction errors, which is the case. SchNet, on the other hand, has several test structures isolated from training data, resulting in higher errors (shown in the ESI†).

Not all structures with a high error are dissimilar in feature space. Models should have learned similar structures and thus should have performed well. A simple, ad hoc geometry descriptor (discussed in the ESI†) applied in Fig. 2B shows that all high-error structures are dissimilar to anything in the data set. SchNet has some difficulty with these structures, which results in a substantial 16.1 kcal mol⁻¹ error. Many-body GAP's 17.6 kcal mol⁻¹ error in $(MeOH)_{16}$ is likely for the same reason. However, GAP uses a local descriptor, making feature space more complicated to analyze. Models under these circumstances were excluded from further analyses (namely, mbSchNet for acetonitrile and mbGAP for methanol).

3.3 20mers

Truncated higher-order contributions could be pertinent for accurate absolute energies, as seen in the previous 16mer data. In practice, relative energy accuracy is of primary importance. Yao *et al.*[59] trained mbML methanol potentials and analyzed their performances on five $(MeOH)_{20}$ isomers. They used a Generative Adversarial Network (GAN) trained on RI-MP2/cc-pVTZ energies with the Coulomb matrix descriptor. Training included 80% of their data sets that contained 844 800 monomers, 74 240 dimers, and 36 864 trimers.
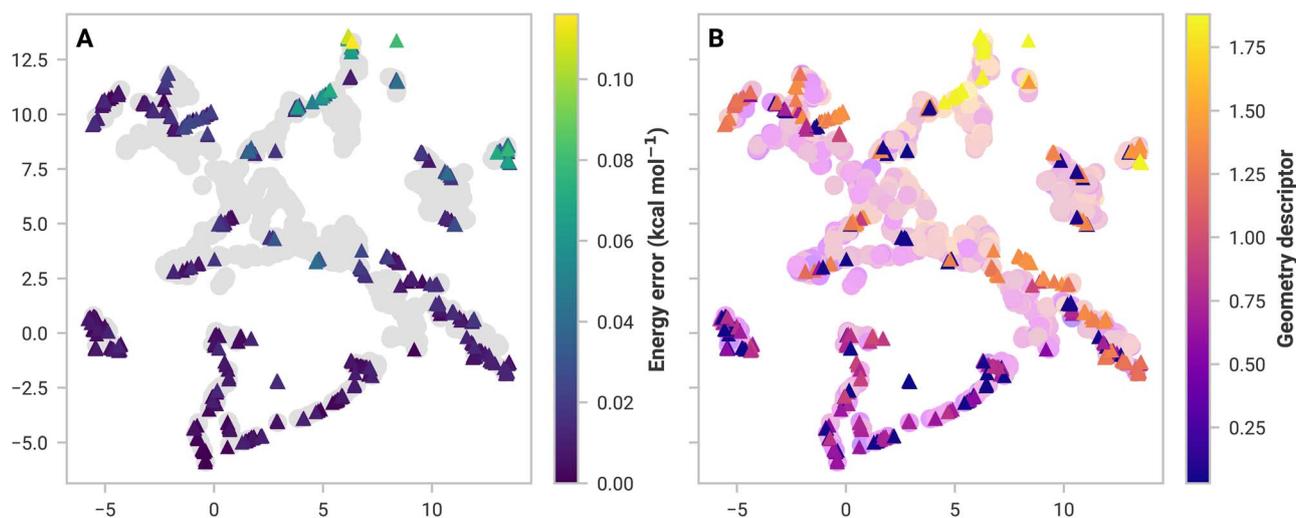

Fig. 2 UMAP embeddings of acetonitrile, 3-body GDML feature space of the training set (circles) and $(MeCN)_{16}$ structure (triangles). Points near each other are similar in high-dimensional feature space. (A) GDML absolute prediction error of 3-body structures from $(MeCN)_{16}$—the maximum error is 0.116 kcal mol⁻¹. (B) Geometry descriptor of each structure. Similar values (*i.e.*, colors) indicate similar geometries.

Table 4 Relative energies (kcal mol^{-1}) of four (MeOH)$_{20}$ with respect to the lowest energy structure (isomer 0). Errors are provided within the parentheses. Best ML potential values are bolded

| | Isomer | | | |
Method	1	2	3	4
RI-MP2[a]	31.0	40.9	50.8	52.0
MBE[a]	27.5	39.6	48.0	48.6
	(−3.5)	(−1.3)	(−2.8)	(−3.4)
mbGAN[a]	26.1	39.8	**49.2**	49.8
	(−4.9)	(−1.1)	(**−1.6**)	(−3.0)
RI-MP2[b]	28.5	38.9	49.9	49.5
mbGDML	**29.1**	**38.9**	51.2	**48.4**
	(**0.6**)	(**0.0**)	(2.2)	(**−1.1**)
mbSchNet	33.6	41.4	52.7	53.0
	(5.1)	(2.5)	(2.8)	(3.5)

[a] RI-MP2/cc-pVTZ, MBE, and mbGAN (trained on 675 840 monomers, 59 392 dimers, and 29 491 trimers) data are from ref. 59. [b] RI-MP2/def2-TZVP data calculated here.

Table 5 Energy MAEs (kcal mol^{-1}) of various sized isomers for mbGDML (many-body global descriptor) and NequIP (local descriptor). MAEs on a per monomer basis are italicized. Best ML potential values are bolded

Solvent	Method	4mers	5mers	6mers	16mer
H$_2$O	mbGDML	0.793	**1.088**	**1.765**	**4.013**
		0.198	*0.218*	*0.294*	*0.251*
	NequIP	**0.727**	1.650	3.609	37.903
		0.182	*0.330*	*0.601*	*2.369*
MeCN	mbGDML	**0.260**	**0.317**	**0.288**	**0.282**
		0.065	*0.063*	*0.048*	*0.018*
	NequIP	1.671	2.116	2.970	28.510
		0.418	*0.423*	*0.495*	*1.782*
MeOH	mbGDML	**1.260**	**1.805**	**2.089**	**5.561**
		0.342	*0.374*	*0.382*	*0.348*
	NequIP	4.006	6.661	7.902	21.732
		1.002	*1.332*	*1.317*	*1.358*

Relative isomer energies of their methods are reported in Table 4. Their mbGAN potential accurately captures the isomer ranking trend within 5 kcal mol^{-1}. mbGDML and mbSchNet (trained on MP2/def2-TZVP) were within 2.2 and 5.1 kcal mol^{-1} of RI-MP2/def2-TZVP calculations on the same (MeOH)$_{20}$ structures. Note that the supersystem calculations here differ from Yao et al.;[59] for example, our calculations predict that isomer 4 is lower in energy than isomer 3.

3.4 Size transferability of local descriptors

As previously mentioned, many ML potentials use local descriptors for size transferability. Recent developments of ML potentials with local descriptors have involved GNNs.[13,14] NequIP uses equivariant, continuous convolutions where edges connect every atom within a cutoff radius.[13] NequIP has achieved remarkable accuracy and data efficiency on the MD17 data set, bulk water, formate dehydrogenation, and amorphous lithium phosphate.

Such models are inherently size transferable, but the accuracy is not typically studied when trained exclusively on small clusters. In theory, these potentials can train on the same data sets here, but instead of n-body interactions, they would use total energies and forces. This would eliminate the need for an MBE framework. We trained NequIP on total energies and forces of 1000 trimers for water, acetonitrile, and methanol to assess this approach. Another 2000 trimers were used as a validation set.

We emphasize that this is an edge case of GNN potentials. If energies and forces of larger structures were readily available, these data would improve size transferability if they were included in the validation set. However, mbGDML models were never exposed to these larger clusters during training since the objective was to reproduce the 1-, 2-, and 3-body PES. Thus, training a NequIP on only trimers represents a straightforward comparison to mbGDML. These models were then tested against the identical isomers discussed above, with the results

shown in Table 5. While NequIP can expectedly extrapolate to larger clusters, the errors are substantially higher than mbGDML. For example, the NequIP error on (H$_2$O)$_{16}$ was more than 33 kcal mol^{-1} higher than mbGDML.

These static cluster results demonstrate that mbGDML is a reasonably accurate, size-transferable force field. The desired level of theory for reference data determines the MBE framework's viability. Training on large clusters or bulk systems is likely more efficient if a lower scaling method is satisfactory. However, mbGDML becomes particularly useful when applications require force fields based on higher-scaling methods. Recovering truncated higher-order contributions would also expectedly improve errors, but explicit 4-body interactions are rather challenging due to high demands on precision and combinatorics.[48,49,60] Electrostatic[61] and more general quantum embedding approximations may be a practical route to avoid calculating higher-order contributions, but they are not considered here.

3.5 Molecular dynamics simulations

While accurate predictions of static clusters are essential, compelling applications for mbGDML would involve molecular simulations. Low energy and force errors are not conclusive of accurate molecular simulations,[62] but experimentally measurable dynamic properties are an alternative and rigorous way to evaluate ML potentials. For example, the radial distribution function (RDF) is a vital bulk property that quantitatively defines liquid structure. Locations and intensities of peaks and valleys represent the solvation shells and liquid ordering. Accurately reproducing reference RDF curves is crucial for a practical size-transferable potential.

Periodic NVT simulations driven by mbGDML force fields were performed at 298.15 K for 10–30 ps in the atomic simulation environment (ASE).[63] Note that NVT simulations could artificially bias intermolecular distances due to the volume constraint. NPT simulations would be a more rigorous metric, but these are not yet implemented in mbGDML, and this will be

the focus of future work. The minimum-image convention was used with cubic boxes with lengths of 16 Å (137 molecules), 18 Å (67 molecules), and 16 Å (61 molecules) for water, acetonitrile, and methanol, respectively. Production trajectories were used to compute all possible RDFs. Some RDF curves are shown in Fig. 3. Water,[64] acetonitrile,[65] and methanol[66,67] reference RDF curves are from neutron diffraction experiments. Results from classical MD simulations[68–74] are also shown in Fig. 3. Note that classical references often include some fitting to empirical data,[68,71–74] whereas mbGDML and others[69,70] run calculations with no explicit empirical fitting. Individual figures of all RDF curves, along with labeled classical references, are shown in the ESI.†

Dispersion and polarization are not always accurately treated with MP2 theory,[75,76] and likewise, the underlying model chemistry (MP2/def2-TZVP) to train mbGDML force fields may not accurately reproduce experimental liquid properties. For example, MP2 yields excellent results for liquid water simulations when appropriate density corrections or basis set error

cancellation schemes are employed,[77,78] but these were not used here. To our knowledge, a thorough investigation has not been performed for liquid acetonitrile and methanol with MP2, so the agreement with experiments is more uncertain. Note that molecular simulations using Kohn–Sham density functional theory (DFT) results in comparable differences in RDFs shown in Fig. 3, depending on the exchange-correlation functional and dispersion treatment used.[79–83]

The simulated RDFs with mbGDML fairly agree with the reference curves. In particular, the water $g_{OO}(r)$ in Fig. 3A agrees remarkably well with experimental data. This is consistent with fragment-based *ab initio* MD (AIMD) simulations.[84,85] However, these AIMD simulations include higher-order contributions through electrostatic embedding. Deviations in the $g_{OH}(r)$ and $g_{HH}(r)$ curves are partially due to the neglect of quantum nuclear effects.[86]

In all cases, acetonitrile peaks from mbGDML are less intense than the reference curves. This indicates that the predicted liquid structure with mbGDML is less ordered than the deuterated neutron diffraction data.[65] Notably, $g_{NN}(r)$ is wide with two distinct peaks that deviate from the experimental reference. However, classical RDFs from the literature can vary substantially. Some classical potentials[70,73] result in a similar $g_{NN}(r)$ shape while others[69,71,72] better resemble the experimental reference.

Methanol simulations appear more challenging for mbGDML. RDF peaks with respect to experimental data are less intense (same as acetonitrile). The shape of $g_{OO}(r)$, Fig. 3C, agrees well with the digitized experimental data. Classical simulations using GROMOS96 and OPLS/AA potentials have significantly more ordered liquid structure.[74] For instance, their $g_{OH}(r)$ peaks are around 1.24 higher in intensity than mbGDML. While the $g_{OO}(r)$ is in good agreement with the experiment beyond 5 Å, the $g_{OH}(r)$ and $g_{HH}(r)$ curves are missing long-range liquid structure. Even though GDML employs a global descriptor, mbGDML is not capturing these long-range interactions. We suspect this is caused by truncations and cutoffs used in the MBE framework.

To summarize, even though the mbGDML models used here only included up to 3-body contributions, they generally predict the liquid structure of water, acetonitrile, and methanol well. Moreover, these force fields automatically include fully flexible molecules and perform no fitting to experimental properties. Further improvements could be made with more expansive training sets and higher-order contributions. For systems without classical parameters, mbGDML can be rapidly trained on relatively small amounts of data and provide valuable dynamical insights for explicitly solvated systems.

4 Conclusions

We have introduced a GDML-driven, many-body expansion framework that enables state-of-the-art size transferability toward molecular simulations of solvents. mbGDML force fields trained on only 1000 1-, 2-, and 3-body interactions accurately modeled small and medium isomers of water, acetonitrile, and methanol. Size-extrapolated predictions on static clusters of up
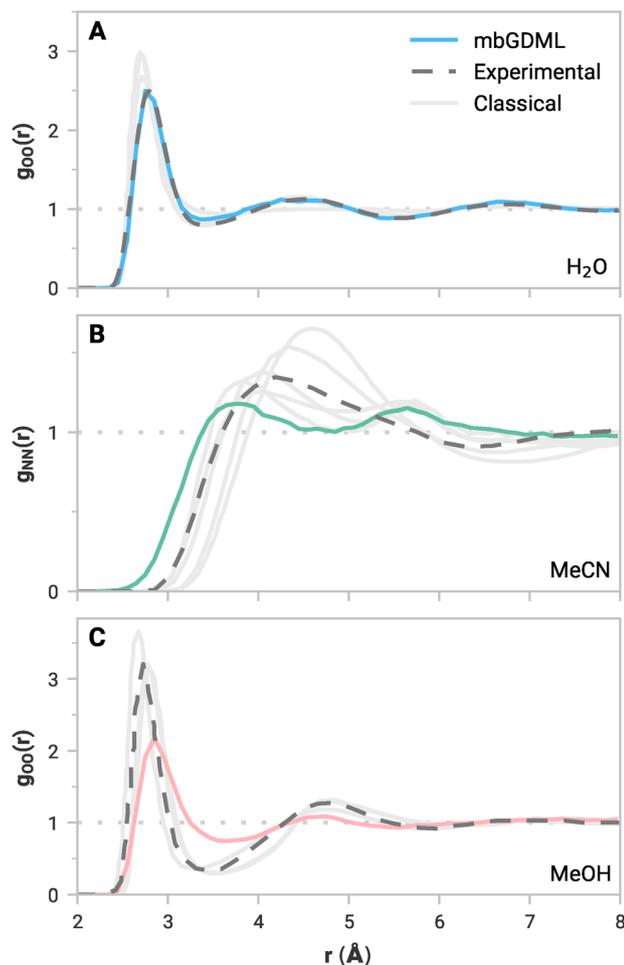

Fig. 3 Simulated RDF curves from NVT MD simulations with mbGDML for (A) $g_{OO}(r)$ in water, (B) $g_{NN}(r)$ in acetonitrile, and (C) $g_{OO}(r)$ in methanol. Reference RDF curves from the literature are shown in dashed gray lines. Examples of classical results in the literature are shown in solid, light gray lines.

to 20 monomers had energy errors of less than 0.38 kcal mol^{-1} per monomer for all three solvents. These results outperform NequIP trained on the same trimer data set by up to 34 kcal mol^{-1} for 16mers. Dynamic simulations of bulk systems using our mbGDML force fields provide semi-quantitative insights while avoiding expensive training data on bulk systems and fitting to experimental data.

It is important to note that the accuracy of mbGDML is generally limited to that of the underlying MBE framework. More extensive and diverse n-body data sets can help minimize mbGDML deviations from the MBE reference. If further accuracy improvements are desired, explicit 4-body ML force fields, classical models, or hybrid methods like MIM and MTA could be required. While these approaches are certainly possible to implement, we focused on providing a proof-of-concept of mbGDML. We thus anticipate promising applications for complex, explicitly solvated systems where high levels of theory are desired.

Data availability

Code for preparing and using many-body ML potentials can be found at **https://github.com/keithgroup/mbGDML** (DOI: **10.5281/zenodo.6270373**). All other code and data supporting this paper are available at **https://github.com/keithgroup/mbgdml-h2o-meoh-mecn** (DOI: **10.5281/zenodo.7802196**) and further detailed in the ESI.†

Author contributions

Alex M. Maldonado: conceptualization, data curation, investigation, methodology, software, validation, visualization, writing; Igor Poltavsky: conceptualization, methodology, funding acquisition, supervision, writing; Valentin Vassilev-Galindo: conceptualization, methodology, supervision, writing; Alexandre Tkatchenko: conceptualization, funding acquisition, supervision, writing; John A. Keith: conceptualization, funding acquisition, supervision, writing.

Conflicts of interest

There are no conflicts to declare.

Acknowledgements

Notes and references

1 J. A. Keith, V. Vassilev-Galindo, B. Cheng, S. Chmiela, M. Gastegger, K.-R. Müller and A. Tkatchenko, *Chem. Rev.*, 2021, **121**, 9816–9872.

2 O. T. Unke, S. Chmiela, H. E. Sauceda, M. Gastegger, I. Poltavsky, K. T. Schütt, A. Tkatchenko and K.-R. Müller, *Chem. Rev.*, 2021, **121**, 10142–10186.

3 V. L. Deringer, A. P. Bartók, N. Bernstein, D. M. Wilkins, M. Ceriotti and G. Csányi, *Chem. Rev.*, 2021, **121**, 10073–10141.

4 G. Pranami and M. H. Lamm, *J. Chem. Theory Comput.*, 2015, **11**, 4586–4592.

5 W. Dawson and F. Gygi, *J. Chem. Phys.*, 2018, **148**, 124501.

6 C. Devereux, J. S. Smith, K. K. Huddleston, K. Barros, R. Zubatyuk, O. Isayev and A. E. Roitberg, *J. Chem. Theory Comput.*, 2020, **16**, 4192–4202.

7 A. S. Christensen, S. K. Sirumalla, Z. Qiao, M. B. O'Connor, D. G. A. Smith, F. Ding, P. J. Bygrave, A. Anandkumar, M. Welborn, F. R. Manby and T. F. Miller, *J. Chem. Phys.*, 2021, **155**, 204103.

8 P. Zheng, R. Zubatyuk, W. Wu, O. Isayev and P. O. Dral, *Nat. Commun.*, 2021, **12**, 7022.

9 F. Musil, A. Grisafi, A. P. Bartók, C. Ortner, G. Csányi and M. Ceriotti, *Chem. Rev.*, 2021, **121**, 9759–9815.

10 A. P. Bartók, R. Kondor and G. Csányi, *Phys. Rev. B: Condens. Matter Mater. Phys.*, 2013, **87**, 184115.

11 A. P. Bartók, M. C. Payne, R. Kondor and G. Csányi, *Phys. Rev. Lett.*, 2010, **104**, 136403.

12 J. Behler and M. Parrinello, *Phys. Rev. Lett.*, 2007, **98**, 146401.

13 S. Batzner, A. Musaelian, L. Sun, M. Geiger, J. P. Mailoa, M. Kornbluth, N. Molinari, T. E. Smidt and B. Kozinsky, *Nat. Commun.*, 2022, **13**, 2453.

14 J. Gasteiger, F. Becker and S. Günnemann, *Advances in Neural Information Processing Systems*, 2021, pp. 6790–6802.

15 Y. Zhai, A. Caruso, S. L. Bore, Z. Luo and F. Paesani, *J. Chem. Phys.*, 2023, **158**, 084111.

16 S. Chmiela, V. Vassilev-Galindo, O. T. Unke, A. Kabylda, H. E. Sauceda, A. Tkatchenko and K.-R. Müller, *Sci. Adv.*, 2023, **8**, eadf0873.

17 H. E. Sauceda, L. E. Gálvez-González, S. Chmiela, L. O. Paz-Borbón, K.-R. Müller and A. Tkatchenko, *Nat. Commun.*, 2022, **13**, 3733.

18 S. Chmiela, A. Tkatchenko, H. E. Sauceda, I. Poltavsky, K. T. Schütt and K.-R. Müller, *Sci. Adv.*, 2017, **3**, e1603015.

19 S. Chmiela, H. E. Sauceda, K.-R. Müller and A. Tkatchenko, *Nat. Commun.*, 2018, **9**, 3887.

20 H. E. Sauceda, S. Chmiela, I. Poltavsky, K.-R. Müller and A. Tkatchenko, *J. Chem. Phys.*, 2019, **150**, 114102.

21 H. E. Sauceda, M. Gastegger, S. Chmiela, K.-R. Müller and A. Tkatchenko, *J. Chem. Phys.*, 2020, **153**, 124109.

22 S. Chmiela, H. E. Sauceda, A. Tkatchenko and K.-R. Müller, *Machine Learning Meets Quantum Physics*, Springer, 2020, pp. 129–154.

23 J. M. Herbert, *J. Chem. Phys.*, 2019, **151**, 170901.

24 M. A. Collins and R. P. A. Bettens, *Chem. Rev.*, 2015, **115**, 5607–5642.

25 V. Babin, C. Leforestier and F. Paesani, *J. Chem. Theory Comput.*, 2013, **9**, 5395–5403.

26 V. Babin, G. R. Medders and F. Paesani, *J. Chem. Theory Comput.*, 2014, **10**, 1599–1607.

27 G. R. Medders, V. Babin and F. Paesani, *J. Chem. Theory Comput.*, 2014, **10**, 2906–2910.

28 M. Veit, S. K. Jain, S. Bonakala, I. Rudra, D. Hohl and G. Csányi, *J. Chem. Theory Comput.*, 2019, **15**, 2574–2586.

29 G. J. O. Beran, *J. Chem. Phys.*, 2009, **130**, 164115.

30 A. Sebetci and G. J. O. Beran, *J. Chem. Theory Comput.*, 2010, **6**, 155–167.

31 L. W. Chung, W. Sameera, R. Ramozzi, A. J. Page, M. Hatanaka, G. P. Petrova, T. V. Harris, X. Li, Z. Ke, F. Liu, *et al.*, *Chem. Rev.*, 2015, **115**, 5678–5796.

32 N. J. Mayhall and K. Raghavachari, *J. Chem. Theory Comput.*, 2011, **7**, 1336–1343.

33 N. Sahu and S. R. Gadre, *Acc. Chem. Res.*, 2014, **47**, 2739–2747.

34 V. Zaverkin, D. Holzmüller, R. Schuldt and J. Kästner, *J. Chem. Phys.*, 2022, **156**, 114103.

35 K. T. Schütt, H. E. Sauceda, P.-J. Kindermans, A. Tkatchenko and K.-R. Müller, *J. Chem. Phys.*, 2018, **148**, 241722.

36 R. M. Richard and J. M. Herbert, *J. Chem. Phys.*, 2012, **137**, 064113.

37 C. Bannwarth, E. Caldeweyher, S. Ehlert, A. Hansen, P. Pracht, J. Seibert, S. Spicher and S. Grimme, *Wiley Interdiscip. Rev.: Comput. Mol. Sci.*, 2020, **11**, e1493.

38 C. Bannwarth, S. Ehlert and S. Grimme, *J. Chem. Theory Comput.*, 2019, **15**, 1652–1671.

39 F. Neese, *Wiley Interdiscip. Rev.: Comput. Mol. Sci.*, 2018, **8**, e1327.

40 F. Neese, *Wiley Interdiscip. Rev.: Comput. Mol. Sci.*, 2012, **2**, 73–78.

41 C. Møller and M. S. Plesset, *Phys. Rev.*, 1934, **46**, 618–622.

42 F. Weigend and R. Ahlrichs, *Phys. Chem. Chem. Phys.*, 2005, **7**, 3297–3305.

43 B. Temelso, K. A. Archer and G. C. Shields, *J. Phys. Chem. A*, 2011, **115**, 12034–12046.

44 A. Malloum, J. J. Fifen and J. Conradie, *Int. J. Quantum Chem.*, 2020, **120**, e26221.

45 S. L. Boyd and R. J. Boyd, *J. Chem. Theory Comput.*, 2007, **3**, 54–61.

46 G. Fonseca, I. Poltavsky, V. Vassilev-Galindo and A. Tkatchenko, *J. Chem. Phys.*, 2021, **154**, 124102.

47 R. M. Richard, B. W. Bakr and C. D. Sherrill, *J. Chem. Theory Comput.*, 2018, **14**, 2386–2400.

48 K.-Y. Liu and J. M. Herbert, *J. Chem. Phys.*, 2017, **147**, 161729.

49 K. U. Lao, K.-Y. Liu, R. M. Richard and J. M. Herbert, *J. Chem. Phys.*, 2016, **144**, 164105.

50 J. F. Ouyang and R. P. Bettens, *J. Chem. Theory Comput.*, 2015, **11**, 5132–5143.

51 J. F. Ouyang, M. W. Cvitkovic and R. P. Bettens, *J. Chem. Theory Comput.*, 2014, **10**, 3699–3707.

52 R. M. Richard, K. U. Lao and J. M. Herbert, *J. Phys. Chem. Lett.*, 2013, **4**, 2674–2680.

53 T. T. Nguyen, E. Székely, G. Imbalzano, J. Behler, G. Csányi, M. Ceriotti, A. W. Götz and F. Paesani, *J. Chem. Phys.*, 2018, **148**, 241725.

54 V. Babin, G. R. Medders and F. Paesani, *J. Phys. Chem. Lett.*, 2012, **3**, 3765–3769.

55 S. Yoo, E. Aprà, X. C. Zeng and S. S. Xantheas, *J. Phys. Chem. Lett.*, 2010, **1**, 3122–3127.

56 K. Remya and C. H. Suresh, *J. Comput. Chem.*, 2014, **35**, 910–922.

57 M. M. Pires and V. F. DeTuri, *J. Chem. Theory Comput.*, 2007, **3**, 1073–1082.

58 L. McInnes, J. Healy and J. Melville, *arXiv*, 2018, preprint, arXiv:1802.03426, DOI: 10.48550/arXiv.1802.03426.

59 K. Yao, J. E. Herr and J. Parkhill, *J. Chem. Phys.*, 2017, **146**, 014106.

60 R. M. Richard, K. U. Lao and J. M. Herbert, *J. Chem. Phys.*, 2014, **141**, 014108.

61 S. K. Reddy, S. C. Straight, P. Bajaj, C. Huy Pham, M. Riera, D. R. Moberg, M. A. Morales, C. Knight, A. W. Götz and F. Paesani, *J. Chem. Phys.*, 2016, **145**, 194504.

62 X. Fu, Z. Wu, W. Wang, T. Xie, S. Keten, R. Gomez-Bombarelli and T. Jaakkola, *arXiv*, 2022, preprint, arXiv:2210.07237, DOI: 10.48550/arXiv.2210.07237.

63 A. H. Larsen, J. J. Mortensen, J. Blomqvist, I. E. Castelli, R. Christensen, M. Dułak, J. Friis, M. N. Groves, B. Hammer, C. Hargus, *et al.*, *J. Phys.: Condens. Matter*, 2017, **29**, 273002.

64 A. K. Soper, *Int. Scholarly Res. Not.*, 2013, **2013**, 279463.

65 E. K. Humphreys, P. K. Allan, R. J. Welbourn, T. G. Youngs, A. K. Soper, C. P. Grey and S. M. Clarke, *J. Phys. Chem. B*, 2015, **119**, 15320–15333.

66 T. Yamaguchi, K. Hidaka and A. K. Soper, *Mol. Phys.*, 1999, **96**, 1159–1168.

67 T. Yamaguchi, K. Hidaka and A. K. Soper, *Mol. Phys.*, 1999, **97**, 603–605.

68 M. W. Mahoney and W. L. Jorgensen, *J. Chem. Phys.*, 2000, **112**, 8910–8922.

69 M. Albertí, A. Amat, F. De Angelis and F. Pirani, *J. Phys. Chem. B*, 2013, **117**, 7065–7076.

70 J. Hernández-Cobos, J. M. Martínez, R. R. Pappalardo, I. Ortega-Blake and E. S. Marcos, *J. Mol. Liq.*, 2020, **318**, 113975.

71 V. A. Koverga, O. M. Korsun, O. N. Kalugin, B. A. Marekha and A. Idrissi, *J. Mol. Liq.*, 2017, **233**, 251–261.

72 M. H. Kowsari and L. Tohidifar, *J. Comput. Chem.*, 2018, **39**, 1843–1853.

73 S. Pothoczki and L. Pusztai, *J. Mol. Liq.*, 2017, **225**, 160–166.

74 K. Khasawneh, A. Obeidat, H. Abu-Ghazleh, R. Al-Salman and M. Al-Ali, *J. Mol. Liq.*, 2019, **296**, 111914.

75 A. Tkatchenko, R. A. DiStasio Jr, M. Head-Gordon and M. Scheffler, *J. Chem. Phys.*, 2009, **131**, 094106.

76 J. Řezáč, C. Greenwell and G. J. Beran, *J. Chem. Theory Comput.*, 2018, **14**, 4711–4721.

77 S. Y. Willow, X. C. Zeng, S. S. Xantheas, K. S. Kim and S. Hirata, *J. Phys. Chem. Lett.*, 2016, **7**, 680–684.

78 M. Del Ben, M. Schönherr, J. Hutter and J. VandeVondele, *J. Phys. Chem. Lett.*, 2013, **4**, 3753–3759.

79 N. Barbosa, M. Pagliai, S. Sinha, V. Barone, D. Alfè and G. Brancato, *J. Phys. Chem. A*, 2021, **125**, 10475–10484.

80 J. Chen and P. H.-L. Sit, *Chem. Phys.*, 2015, **457**, 87–97.

81 N. Sieffert, M. Bühl, M.-P. Gaigeot and C. A. Morrison, *J. Chem. Theory Comput.*, 2013, **9**, 106–118.

82 M. J. McGrath, I.-F. W. Kuo and J. I. Siepmann, *Phys. Chem. Chem. Phys.*, 2011, **13**, 19943–19950.

83 J.-W. Handgraaf, T. S. van Erp and E. J. Meijer, *Chem. Phys. Lett.*, 2003, **367**, 617–624.

84 J. Liu, X. He, J. Z. Zhang and L.-W. Qi, *Chem. Sci.*, 2018, **9**, 2065–2073.

85 S. Y. Willow, M. A. Salim, K. S. Kim and S. Hirata, *Sci. Rep.*, 2015, **5**, 14358.

86 A. Eltareb, G. E. Lopez and N. Giovambattista, *Phys. Chem. Chem. Phys.*, 2021, **23**, 6914–6928.